TECHNICAL MEMORANDUM

713

Global mass fixer algorithms for conservative tracer transport in the ECMWF model

M. Diamantakis and J. Flemming

Research Department

October 2013

European Centre for Medium-Range Weather Forecasts
Europäisches Zentrum für mittelfristige Wettervorhersage
Centre européen pour les prévisions météorologiques à moyen terme

Series: ECMWF Technical Memoranda

A full list of ECMWF Publications can be found on our web site under:
http://www.ecmwf.int/publications/

Contact: library@ecmwf.int

European Centre for Medium-Range Weather Forecasts
Shinfield Park, Reading, RG2 9AX, England

Contents

Abstract

Various mass fixer algorithms have been implemented in the ECMWF Integrated Forecasting System (IFS). These algorithms are applied on tracer fields to maintain a globally mass conserving solution during the semi-Lagrangian advection step.

In this report, the mass conservation properties of IFS are discussed and a description of the implemented mass fixer algorithms is given. Emphasis has been placed in implementing schemes that, despite being primarily global in nature, adjust the solution mostly in regions where the advected field has large gradients and therefore interpolation (transport) error is assumed larger.

The algorithms have been tested in weather forecast, idealised and atmospheric dispersion cases. Results show that, in the context of 10-day weather forecasts, when these fixers are applied on specific humidity and cloud fields the impact on predictive skill is mostly neutral. Global mass tracer conservation is achieved without deteriorating the solution accuracy. However, for longer forecast timescales or for forecasts in which correlated species are transported, there are indications that the mass fixer approach may improve IFS forecasts.

The above results are valid for hydrostatic regimes. Further testing is needed to quantify more accurately the impact of mass fixers on non-hydrostatic scales as well as on IFS based prediction systems for atmospheric composition and climate forecasts. Based on current results we make recommendations on which options to use for specific cases.

1 Introduction

A well known drawback of semi-Lagrangian transport schemes, such as the one used by IFS, is that they do not formally conserve mass. In the absence of sources and sinks, between the beginning and the end of each timestep, the total model mass differs by a very small amount. This difference, although is not significant for NWP forecast timescales, may accumulate in a long run. The total mass of air or a tracer field may eventually drift significantly affecting the quality of the forecast.

As NWP models become more complex, the number of tracers increases and the requirement for conservative schemes becomes more important. Furthermore, as the resolution increases and we slowly progress towards cloud resolving scales it becomes increasingly desirable from the parametrization point of view to have a mass conserving advection scheme as this may improve further the simulation of cloud processes.

There is a class of semi-Lagrangian schemes, the so called inherently conserving schemes, which are able to achieve global, local and consistent mass conservation for tracer and air-mass fields. Two typical examples are SLICE Zerroukat and Allen (2012) and CSLAM Lauritzen et al. (2010). Such schemes are essentially an application of a finite-volume type discretization approach on the semi-Lagrangian continuity equation. However, they are complex to implement in a three-dimensional setup which includes orography and they are expensive. The computing cost can easily double compared with traditional semi-Lagrangian methods. Inherently conserving schemes is an active area of research. They are not currently used in forecasting operations but further improvements may change this, especially for applications when multiple tracers are transported. An example of a very recent development is given in the paper by Sørensen et al. (2013).

An alternative low computational cost approach is the so called "mass fixer" algorithm. The practice is to perform first the standard semi-Lagrangian advection step (find departure points, interpolate the advected field to them) and then to correct the solution in order to satisfy global mass conservation.

There is a range of mass fixer algorithms published in the literature. They distribute the global mass loss

or gain in different ways. The simplest mass fixers correct the solution uniformly by simply scaling each grid-point value with the ratio of the global mass before and after advection[1]. A criticism to this approach is that in some areas the fixer may be changing the solution even though there is no need to do so. More sophisticated algorithms attempt to compute a correction which is proportional to the smoothness of the solution. A larger correction is computed in areas where the solution has large gradients and therefore the error is larger and a very small correction where the solution is smooth and the error is small. The aim of this report is to describe tracer mass fixer algorithms that were recently implemented in IFS and discuss results from different application areas appropriate for applying these fixers. Availability of globally mass conserving schemes for tracers can be an important addition to IFS based prediction systems such as the EC-Earth climate model or atmospheric composition forecast systems where aerosols, greenhouse and reactive gases are transported.

2 Air and tracer global mass conservation in IFS

In a 10-day IFS forecast, at T1279 horizontal resolution (approximately 16km in grid-point space) and 137 levels in the vertical, the total model air mass is approximately increasing by less than 0.01% of its initial value. The formulation of the continuity equation, based on Ritchie and Tanguay (1996) scheme (see also ECMWF, 2012, section 3.6.2), plays an important role into achieving this accuracy. Orography is removed from the advected mass field resulting in a much smoother field which can be accurately interpolated to the Lagrangian-grid (departure points).

Global conservation errors in tracer advection are larger and depend on the smoothness of the field. For example, smoother fields such as ozone and specific humidity have much smaller conservation errors than fields with sharp features such as cloud fields. This is demonstrated in Fig.1 where the global mass conservation error is displayed for ozone, specific humidity (Q), liquid cloud water content (CLWC), cloud ice water content (CIWC). A conservative scheme would have been represented in this plot by a line identical to the horizontal 0-axis; the closer to the horizontal axis a curve is the smaller the mass conservation error. In these experiments, *parametrizations have been switched off* to isolate sources and sinks and allow testing the performance of the advection scheme in realistically complex terrain. Two sets of results have been included: (i) using quasi-cubic ECMWF interpolation, Ritchie et al. (1995), with a quasi-monotone limiter and (ii) using linear interpolation (indicated with LIN in plots). The former choice is used in IFS operationally for Q while the later is used operationally for the rougher cloud fields. The experiments are run at different horizontal and vertical resolutions: (i) T159 L60 i.e. T159 in the horizontal with 60 levels in the vertical (ii) T159 L91 (iii) T1279 L91 and (iv) T1279 L137.

To quantify the impact of different resolutions and interpolation schemes, we shall define the global mass conservation error for a tracer ϕ, expressed as a percentage of its initial mass:

$$E_\phi = 100 \times \frac{M_t^\phi - M_0^\phi}{M_0^\phi}$$

where, M_0^ϕ, M_t^ϕ is the initial and current step global tracer mass. E_ϕ is plotted in Fig. 1. To allow direct comparisons of the per timestep mass conservation error, the four top forecasts in Fig. 1 have been run for the same number of timesteps. At coarse horizontal resolution (T159) the timestep is 6 times longer (60 mins) than the corresponding timestep for high resolution (T1279).

The overall impression from these results is that the global mass conservation error per timestep tends

[1]This is used in IFS when long time integrations take place in order to correct the total model air-mass.

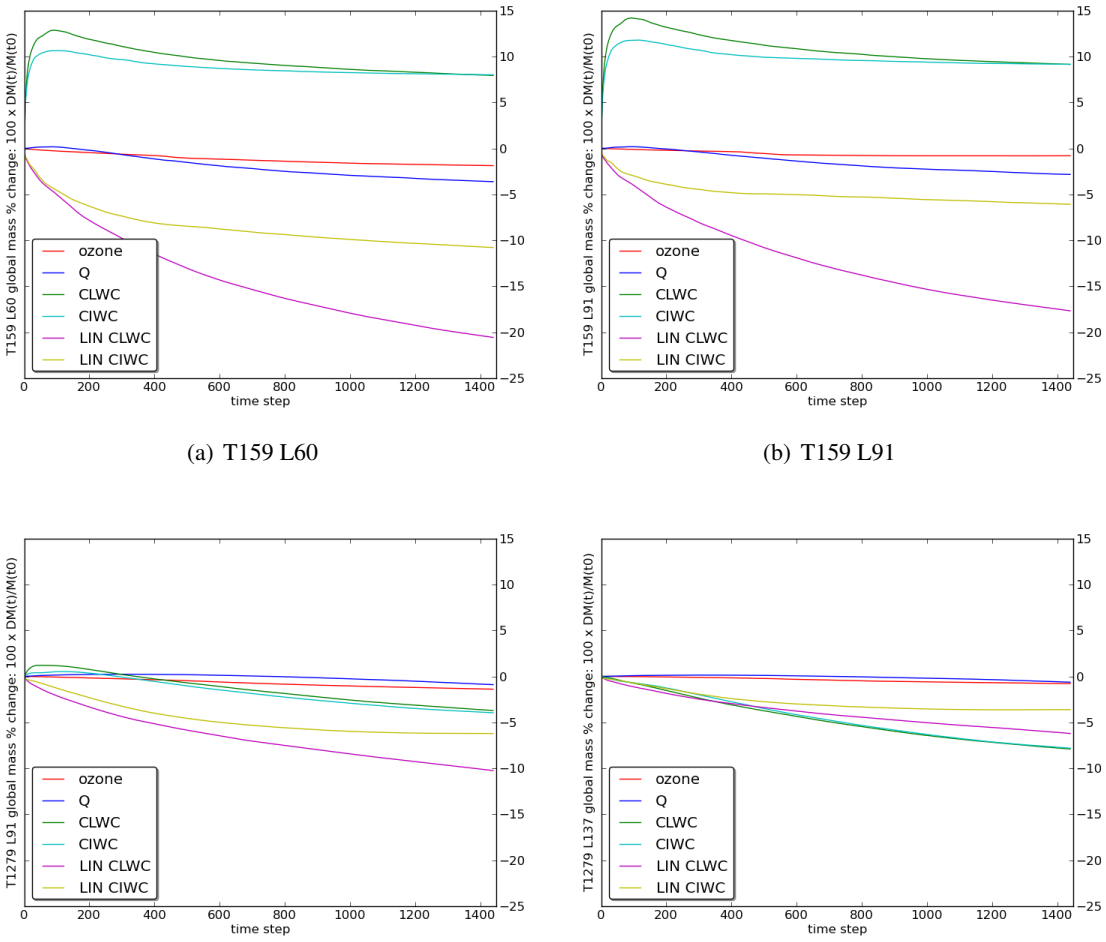

(a) T159 L60

(b) T159 L91

(c) T1279 L91

(d) T1279 L137

Figure 1: Mass conservation error as a percent of initial global mass for ozone, Q, CLWC,CIWC at different resolutions.

to decrease as the resolution increases. This may not be a precise statement for every tracer but gives a strong indication of a reduction of the error per timestep as resolution is refined especially when this error is large. So apart of the expected improvement in forecasting accuracy obtained with increased resolution an improvement in global mass conservation is achieved as well. For cubic interpolation, increase of horizontal resolution results to a noticeable reduction of the global tracer mass error, in particular for CLWC, CIWC. Increasing the vertical resolution seems to have a small positive impact for the smoother fields (Q, ozone). For the linearly interpolated fields, increasing vertical resolution, leads to a reduction of their global mass error. Increasing horizontal resolution improves 'LIN CLWC' but leaves relatively un-affected 'LIN CIWC' which is the most localised and least smooth. Finally, no improvement was found when the timestep length was reduced.

3 Implemented Mass Fixers

The transport problem we consider here is advection of a scalar field ϕ_χ which represents the mass mixing ratio of a tracer:

$$\frac{D\phi_\chi}{Dt} = S, \quad \phi_\chi = \rho_\chi/\rho \tag{1}$$

where ρ_χ, ρ are the tracer and air density respectively and S represents sources or sinks that may be present. Consider semi-Lagrangian time-stepping from t to $t+\Delta t$:

$$\phi_\chi^{t+\Delta t} = \phi_{\chi,d}^{t} + \Delta t\, S$$

where d denotes the departure point computed by the trajectory algorithm and $\phi_{\chi,d}^t$ is obtained by interpolating the known field ϕ_χ^t at the computed departure point. If $S=0$ then the global volume integral of $\rho\phi_\chi$ at t and $t+\Delta t$ (on the model grid) should not change as this represents the total mass of χ and the only process operating is advection (transport). However, in practice, as the interpolation scheme generates errors this global conservation law is violated.

Global mass fixers of different sophistication are described in the published literature for semi-Lagrangian transport models. In general, any mass fixer will compute the global mass conservation error of the advection step. Then a small correction is computed for each grid-point in such a way that this global error is eliminated. In the simplest version of the proportional or multiplicative fixer of Rasch and Williamson (1990), each grid-point value is multiplied by the ratio of the mass before and after advection. Here, we will focus on the more local algorithms. In particular, the following algorithms will be discussed: (i) Bermejo and Conde (2002) scheme (ii) Priestley (1993) (iii) MacGregor (2011) and (iv) Zerroukat (2010) scheme. The first two can preserve quasi-monotonicity while this is not true for the last two. These algorithms have been implemented in IFS and will be summarised in the following paragraphs. It should be noted that their implementation is three-dimensional given that semi-Lagrangian advection in IFS is fully three-dimensional.

To describe these different fixers, as implemented in IFS, some notation needs to be first introduced. Assume K model levels in the vertical, starting from the top of the atmosphere and ending on the surface, each one having N grid-points. Each grid-box has horizontal surface area A_j and height Δz_{jk} where z_{jk} denotes the height of the j^{th} model grid-point of the k^{th} level. The total mass of a tracer χ with mass mixing ratio $\phi = \rho_\chi/\rho$ where ρ is the air-density field is:

$$M = \sum_{j=1}^{N} A_j \sum_{k=1}^{K} \rho_{\chi,jk}(-\Delta z_{jk}) = \sum_{j=1}^{N} A_j \sum_{k=1}^{K} \phi_{jk}\frac{\Delta p_{jk}}{g}, \quad \Delta z_{jk} = z_{jk} - z_{j,k-1} < 0,\ \Delta p_{jk} = p_{jk} - p_{j,k-1} > 0$$

where the hydrostatic approximation (valid in IFS) $\Delta p = -\rho g \Delta z$ has been used.

During the advection step, a tracer field ϕ^0 (i.e. the field before the advection step takes place) is interpolated to the departure point field (Lagrangian grid) and changes to ϕ^* while its total mass changes from M^0 to M^*:

$$M^0 = \sum_{j=1}^{N} A_j \sum_{k=1}^{K} \phi_{jk}^0 \frac{\Delta p_{jk}^0}{g}, \quad M^* = \sum_{j=1}^{N} A_j \sum_{k=1}^{K} \phi_{jk}^* \frac{\Delta p_{jk}^*}{g}. \tag{2}$$

Use of Δp^*_{jk} in (2) reflects the change of the surface pressure field due to advection. Mass fixers aim correcting ϕ^* so that a new field is derived which has a total mass equal to M^0.

3.1 Bermejo and Conde (BC) scheme

Bermejo and Conde (2002) algorithm is derived by a variational principle. It computes a new quasi-monotone field minimizing its distance from the original one subject to the constraint of global mass conservation. The correction added at each grid point depends on an estimate of the interpolation error. The global norm of this correction field has the smallest possible magnitude that can give mass conservation and monotonicity. In the original publication, the scheme was tested on idealised 2-dimensional cases of advection. Here it has been implemented in IFS in 3D mode and has been tested on active meteorological fields.

Let ϕ^1 be the field which minimizes the square of the weighted norm:

$$\min_{\phi^1} \|\phi^1 - \phi^*\|^2_w = \frac{1}{2}\sum_{j=1}^{N} A_j \sum_{k=1}^{K} \frac{\left(\phi^1_{jk} - \phi^*_{jk}\right)^2}{w_{jk}} \frac{\Delta p^*_{jk}}{g} \tag{3}$$

subject to

$$\sum_{j=1}^{N} A_j \sum_{k=1}^{K} \phi^1_{jk} \frac{\Delta p^*_{jk}}{g} = M^0$$

where w_{jk} a non-negative weighting factor ($w_{jk} = 0$ simply means that the corresponding grid-point value is not altered and is not included in the cost function). A solution to (3) is found using a Lagrange multiplier approach. The cost function

$$E(\phi^1, \lambda) = \frac{1}{2}\sum_{j=1}^{N} A_j \sum_{k=1}^{K} \frac{\left(\phi^1_{jk} - \phi^*_{jk}\right)^2}{w_{jk}} \frac{\Delta p^*_{jk}}{g} - \lambda \left(\sum_{j=1}^{N} A_j \sum_{k=1}^{K} \phi^1_{jk} \frac{\Delta p^*_{jk}}{g} - M^0 \right),$$

is defined seeking a pair of values $\left(\phi^1, \lambda\right)$ such that:

$$\frac{\partial E}{\partial \phi^1_{jk}} = 0, \quad \frac{\partial E}{\partial \lambda} = 0.$$

Solving these two equations we obtain:

$$\phi^1_{jk} = \phi^*_{jk} - \lambda w_{jk}, \quad \lambda = \frac{\delta M}{\sum_{j=1}^{N} A_j \sum_{k=1}^{K} w_{jk} \frac{\Delta p^*_{kj}}{g}}, \quad \delta M = M^* - M^0 \tag{4}$$

where the weight w_{jk} depends on the solution smoothness and here is chosen to be proportional to the difference between the quasi-cubic, quasi-monotone interpolated field ϕ^* and the linear one ϕ^L:

$$w_{jk} = \max\left[0, sgn(\delta M)\left(\phi^*_{jk} - \phi^L_{jk}\right)^p\right]. \tag{5}$$

The above weights are used to compute a "local correction", i.e. the global mass surplus or deficit is distributed unevenly to different grid-points depending on the smoothness of the solution which is measured by the difference between a high and a low order interpolant. For the IFS implementation, p

was set to 1 as testing didn't show any benefit in using the recommended in the paper value $p = 3$. In fact, higher values led to sharper, bigger size increments which is not desirable from the model stability point of view.

3.2 Zerroukat's (ZE) scheme

The Bermejo and Conde fixer in IFS can also be run in a mode that corresponds to a version of the Zerroukat (2010) fixer. This leads to smoother correction fields. The drawback is that quasi-monotonicity or positive-definiteness cannot be guaranteed. Here an implementation of this scheme is discussed which uses the same measure to assess the solution smoothness as the Bermejo and Conde scheme, i.e. the difference between a high order scheme (cubic Lagrange interpolation) and a low order scheme (linear interpolation).

Using the notation introduced earlier, the Zerroukat fixer corrects each grid-point value as follows:

$$\phi^1_{jk} = \phi^*_{jk} - \gamma_{jk}\delta M, \quad \delta M = M^* - M^0, \quad \gamma_{jk} = \frac{|\phi^*_{jk} - \phi^L_{jk}|^p}{\sum_{j=1}^{N} A_j \sum_{k=1}^{K} |\phi^*_{jk} - \phi^L_{jk}|^p \frac{\Delta p^*_{jk}}{g}} \tag{6}$$

where M^0, M^* are defined by (2) and again $p = 1$ is sufficient for practical purposes. If

$$\sum_{j=1}^{N} A_j \sum_{k=1}^{K} \gamma_{jk} \frac{\Delta p^*_{jk}}{g} = 1$$

holds then global mass conservation is guaranteed:

$$\sum_{j=1}^{N} A_j \sum_{k=1}^{K} \phi^1_{jk} \frac{\Delta p^*_{jk}}{g} = M^0.$$

It is worth noticing that equation (6) can be re-written in a form that resembles (4):

$$\phi^1_{jk} = \phi^*_{jk} - \lambda w_{jk}, \quad \lambda = \frac{\delta M}{\sum_{j=1}^{N} A_j \sum_{k=1}^{K} w_{jk} \frac{\Delta p^*_{jk}}{g}}, \quad \delta M = M - M^0, \quad w_{jk} = |\phi^*_{jk} - \phi^L_{jk}|^p. \tag{7}$$

This implies that the derived field ϕ^1 is also a solution of the minimization problem (3). One difference between (4) and (7) is in the construction of the weight w_{jk}. Using the unlimited $w_{jk} = |\phi^*_{jk} - \phi^L_{jk}|^p$ means that all grid-points will be corrected. The sign of the increment is determined by the sign of δM (which determines the sign of λ): for $\delta M > 0$ (surplus) $\phi^1_{jk} \leq \phi_{jk}$ $\forall j,k$ and for $\delta M < 0$ (deficit) $\phi^1_{jk} \geq \phi_{jk}$ $\forall j,k$. However, as this one-directional correction is not limited as in the Bermejo and Conde case, it is possible that a new minimum or maximum value may be generated. In practice, if a quasi-monotone scheme is used for advection this happens in a small percentage of grid-points (depends on resolution and smoothness of field, often less than 0.5% but sometimes can go up to 3%).

3.3 Priestley's (PR) scheme

Priestley (1993) is a well known mass fixing scheme. Its objective is to compute a globally conserving monotone solution by blending the original high order with a low order solution thereby departing as

little as possible from the high order one. This is equivalent to finding the highest possible values for the weights α_{jk} such that the "blended" field:

$$\phi^1_{jk} = \alpha_{jk}\left(\phi^*_{jk} - \phi^L_{jk}\right) + \phi^L_{jk}, \quad 0 \leq \alpha_{jk} \leq 1$$

satisfies:

$$\min\left(\left\{\phi^0, j, k\right\}, \phi^L_{jk}\right) \leq \phi^1_{jk} \leq \max\left(\left\{\phi^0, j, k\right\}, \phi^L_{jk}\right), \quad \sum_j A^N_{j=1} \sum_{k=1}^{K} \phi^1_{jk} \frac{\Delta p^*_{jk}}{g} = M^0 \tag{8}$$

where $\left\{\phi^0, j, k\right\}$ denotes the set of ϕ-field values (before advection takes place) at grid-points surrounding the (j,k) departure point and ϕ^*, ϕ^L the cubically and linearly interpolated field at the departure point respectively. The two conditions in (8) ensure conservation and monotonicity. The requirement for "highest possible" α-values is an accuracy requirement: ensures that the final solution is as close as possible to the original high order interpolation field. In regions where the solution is smooth the blended scheme is weighted towards the higher order solution while in regions with low degree of smoothness it is blended towards the linear solution. A good step-by-step algorithmic description of Priestley's algorithm is given in the appendix of Gravel and Staniforth (1994) and will not be repeated here. This is an iterative scheme. However, if a quasi-monotone interpolation limiter is used before this algorithm is applied, such as the one by Bermejo and Staniforth (1992) then IFS tests show it converges fast often in a single iteration.

3.4 Mac Gregor's (JMG) scheme

MacGregor (2011) scheme, a mass fixer used in the climate model CCAM (Conformal-Cubic Atmospheric Model), can be applied to any interpolation technique including linear as opposed to the fixers considered so far which both require that the field is advected using a high order interpolant. An additional virtue of this scheme is that it is very cheap. However, it cannot guarantee monotonicity but only positive definiteness. Furthermore, it differs from the other algorithms examined here, as it does not use a local smoothness criterion to assess how much to correct at each grid-point. At each timestep it computes a global diagnostic which judges the overall ability of the advection scheme to accurately translate fields. Nevertheless it does not correct by the same proportion each grid-point but is using instead two different scaling factors: one for points that have positive advective increments and one for points that have negative advective increments. It tends to amplify the solution when there is damping and suppress when there is amplification. The IFS implementation of this fixer is fully three-dimensional given that semi-Lagrangian advection is applied in all three dimensions (on a reduced Gaussian grid) while in CCAM a total variation diminishing (TVD) scheme is used for the vertical advection.

Using the previously introduced notation the algorithm can be described as follows:

Step 1 Compute total mass before and after advection M^0, M^* as in (2).

Step 2 Let a minimum allowed value ϕ^{min}. Scan each grid point, compute and store:

$$\Delta\phi^+_{jk} = \max\left(0, \Delta\phi_{jk}\right), \quad \Delta\phi^-_{jk} = \min\left(0, \Delta\phi_{jk}\right)$$

where

$$\Delta\phi_{jk} = \max\left(\phi^*_{jk}, \phi^{min}_{jk}\right) - \frac{\Delta p^0_{jk}}{\Delta p^*_{jk}} \phi^0_{jk}$$

Step 3 Compute total positive and negative increments and their ratio :

$$\Delta M^{+} = \sum_{j=1}^{N} A_j \sum_{k=1}^{K} \frac{\Delta p^0_{jk}}{g} \Delta \phi^{+}_{jk}, \qquad \Delta M^{-} = \sum_{j=1}^{N} A_j \sum_{k=1}^{K} \frac{\Delta p^*_{jk}}{g} \Delta \phi^{-}_{jk},$$
$$r = -\frac{\Delta M^{-}}{\Delta M^{+}}$$

Step 4 Set $\alpha_\phi = \min(r, \sqrt{r})$ and update:

$$\phi^1_{jk} = \frac{\Delta p^0_{jk}}{\Delta p^*_{jk}} \phi^0_{jk} + \alpha_\phi \Delta \phi^{+}_{jk} + \frac{1}{\max(1, \alpha_\phi)} \Delta \phi^{-}_{jk}$$

The last step is equivalent to:

$$\phi^1_{jk} = \begin{cases} \frac{\Delta p^0_{jk}}{\Delta p^*_{jk}} \phi^0_{jk} + \alpha_\phi \Delta \phi^{+}_{jk} + \Delta \phi^{-}_{jk}, & r \leq 1 \\ \frac{\Delta p^0_{jk}}{\Delta p^*_{jk}} \phi^0_{jk} + \alpha_\phi \Delta \phi^{+}_{jk} + \frac{1}{\alpha_\phi} \Delta \phi^{-}_{jk}, & r > 1 \end{cases}$$

and implies that the increment is scaled by a factor α_ϕ which reduces positive increments when their total mass exceeds the total mass of the negative increments. When the opposite is true then positive increments will be amplified and negatives will reduce in magnitude. The new field satisfies the global mass conservation constraint:

$$\sum_{j=1}^{N} A_j \sum_{k=1}^{K} \phi^1_{jk} \frac{\Delta p^*_{jk}}{g} = M_0.$$

3.5 The quasi-monotone limiter

For the tests presented in the following section two forms of the quasi-monotone Bermejo and Staniforth (1992) max-min limiter for cubic interpolation will be used:

(i) "the default" limiter or filter: in this version the scheme is applied immediately after each 1D cubic interpolation (in longitude, latitude, height) takes place. So, the steps taken are: interpolate in longitude and then apply 1D limiter on the interpolated field. Repeat this action for each of the remaining two interpolations (in latitude, height).

(ii) the standard Bermejo and Staniforth (1992) limiter: this shall be called **BS** limiter or filter. In this case the limiter is applied after all three interpolations have finished, i.e. this is limiting in 3D at once.

4 Testing of mass fixers in IFS

The following naming convention will be used for the mass fixers: (i) **BC** will denote the Bermejo and Conde (2002) scheme (ii) **PR** is the Priestley (1993) algorithm (iii) **PRqm** is a slightly modified version of Priestley's algorithm which acts on a quasi-monotone limited cubic-Lagrange field (the original version acts on a cubic-Lagrange unlimited field) (iv) **JMG** is the MacGregor (2011) scheme and (v) **ZE** is a version of Zerroukat (2010) scheme briefly analysed above. The term quasi-monotone used here

implies that the interpolation formula is locally monotone, i.e. in the vicinity of the departure point the interpolation curve (or multidimensional surface) passing from the departure point field value and the field values of points surrounding the departure point does not generate new minima or maxima. Furthermore, the term "cubic interpolation" will imply the quasi-cubic interpolation scheme used by IFS (linear interpolation along the edges of the stencil, fully cubic in the interior, see Ritchie et al., 1995).

In Fig. 2 the global conservation error during the advection of Q and CLWC with and without mass fixer is displayed. The test here is identical to the one that corresponds to the results of Fig. 1 i.e. there are no sources or sinks of tracer mass. It is run at operational resolution T1279 in the horizontal with 137 levels in the vertical. For brevity we display only results from **BC** and **PR** schemes. The same result is obtained with the remaining mass fixer. This plot shows that the mass fixer results in a globally mass conserving solution[2].

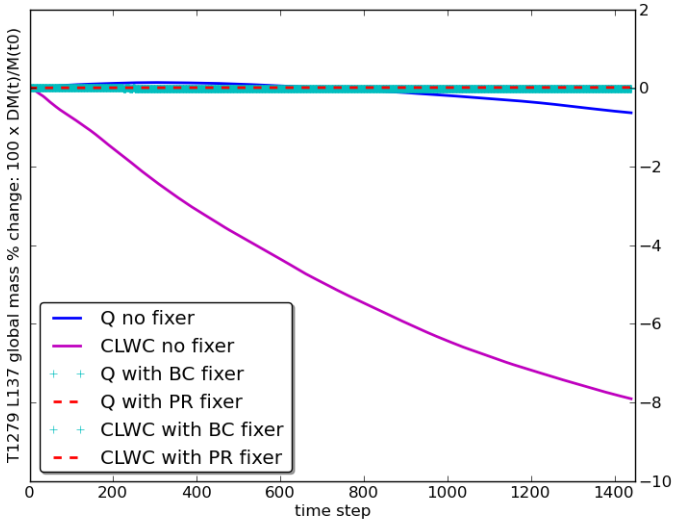

Figure 2: Mass conservation errors as a percentage of initial global mass for Q, CLWC at T1279 L137 resolution forecast with/without mass fixers.

The local behaviour of the mass fixers, applied on Q is demonstrated in Figs. 3 to 5. Cubic interpolation is used for the advection of this field and parametrizations have been switched on. A single timestep increment from the fixer, at $t = 24$ hrs and at a model level which over flat terrain is near the 700 hPa pressure level, is compared with the field itself. Results show that the computed increments are at least 3 orders of magnitude smaller than their corresponding field magnitude. The sign is negative due to the fact that at this stage of the forecast, advection increases mass and the fixer has to remove the surplus. Another observation is that fixers are acting mainly on areas where large gradients are present where interpolation is expected to be less accurate. In areas where the field is smooth the correction is very

[2]When the mass fixer is applied, the difference in the total mass of a tracer before and after advection is always close to machine precision. However, due to the semi-implicit correction of surface pressure which is applied at the end of the timestep, the global mass integral after this correction may not exactly conserve, even if the advection step is perfectly conserving and there are no sources or sinks of mass. Surface pressure is modified which results in a modification of the vertical placement of the levels which in turn affects vertical (column) integration. This is a separate problem, not addressed by these mass fixers which are coded to make the semi-Lagrangian step globally conserving. In order to obtain mass conservation in machine precision a further small adjustment to account for the change in pressure is required at the end of the timestep after the semi-implicit correction. However, for practical purposes as we can see from this plot the mass conservation error is essentially 0.

small regardless of the field magnitude.

It is evident that increments computed by **PR** (see Fig. 4b) differ significantly from the other fixers. This is because this algorithm computes a quasi-monotone and conservative solution iteratively starting from a cubic interpolated field. In the tests presented here it usually takes 3-4 iterations to converge. During this iterative process both positive and negative increments will be computed to satisfy local monotonicity. Mass has to be removed from overshooting points (negative increment) and added at undershooting points (positive increment). This is not the case with **PRqm** which starts with a quasi-monotone field having no undershooting or overshooting points (see Fig. 4b) and therefore the only action that the algorithm needs to take is to restore global mass conservation. Regarding the remaining fixers it is worth mentioning that: (i) **ZE** produces the smallest in magnitude increments but these are more widespread (ii) **BC** and **PRqm** are similar and (iii) **JMG** produces slightly different patterns than the previous two fixers. As expected, the quasi-monotone schemes did not produce any overshoots or undershoots. A very small percentage of undershoots ($< 0.01\%$ of total points) was found with **JMG** but no negative values were created. This percentage was larger in the **ZE** fixer for the cloud fields, exceeding slightly 1.5%, while it was of similar magnitude for Q ($\approx 0.01\%$). Most of these undershoots generated negative values.

A zonally and 24 hrs time-averaged vertical cross section for Q is compared with corresponding cross-sections of increment diagnostics in Fig. 6. The average increment is 4-5 orders of magnitude smaller than the magnitude of the field itself. It is concentrated in areas where large amounts of humidity are present. It is interesting to notice how similar the zonally and time averaged increments are for **BC**, **ZE** and **PRqm**. The fact that their difference is small means that the different algorithms converge roughly to the same solution. Larger differences can be noticed when any of the previous three fixers is compared with **JMG** and even larger with **PR** (for reasons explained in previous paragraph).

In the plots presented here specific humidity was chosen to examine the local behaviour of mass fixers. This choice was made due to the meteorological importance of this tracer field and given that it includes regions that are relatively smooth as well as regions with large gradients. The same plots have been produced for the rougher cloud fields as well but they are not included here as our conclusions are also valid for them. However, it is interesting to use CLWC increments as a diagnostic for demonstrating the step by step behaviour of the mass fixers. This is shown in Fig. 7 where the scaled global rms and max norms of the of CLWC fixer (absolute) increments are displayed. These are scaled to be the fraction (percentage) of the rms global norm of the advected CLWC field which is representative to its mean value. The plot clearly shows that the smallest increments are computed by **ZE** fixer, followed by **BC** and **PRqm** while as expected and explained before **PR** computes the largest increments. **JMG** increments are in the middle between **PR** and **ZE**.

Finally, to assess the computational cost of the fixers, 10-day forecast tests with the high resolution control (T1279 L137) have been done applying the fixers on Q, CLWC, CIWC, CRWC (cloud rain water content) and CSWC (cloud snow water content). The extra CPU time consumed by these algorithms is shown in Table 1. As expected Priestley's scheme is the most expensive and MacGregor's the cheapest. All algorithms are parallelized using MPI and openMP.

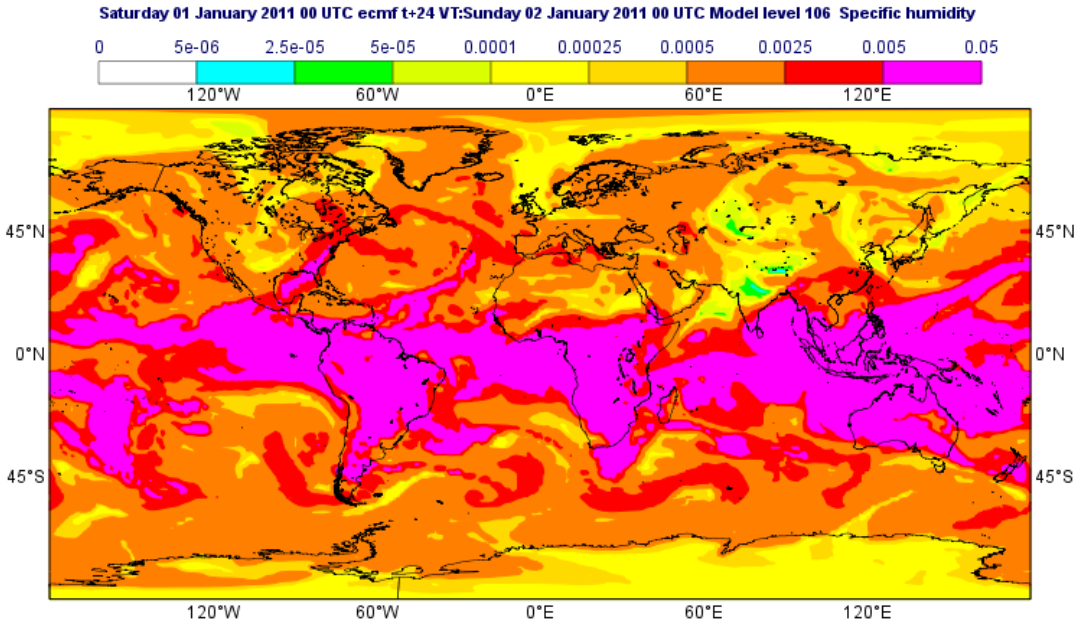

(a) Q field

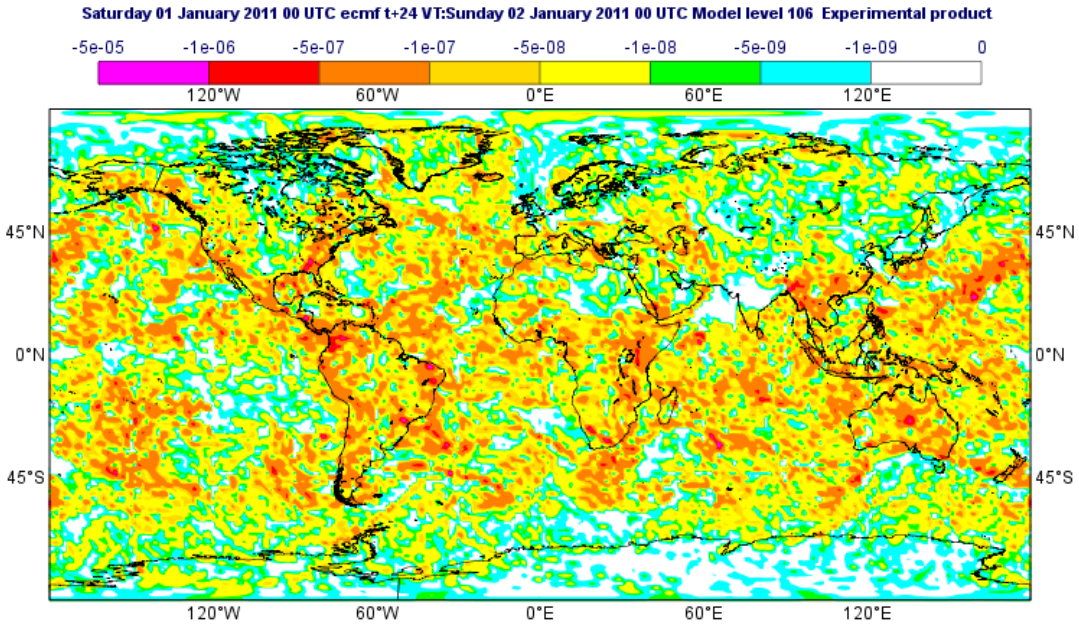

(b) BC fixer

Figure 3: Q and BC fixer Q increment at t+24 and 700 hPa height from a T1279 L137 forecast.

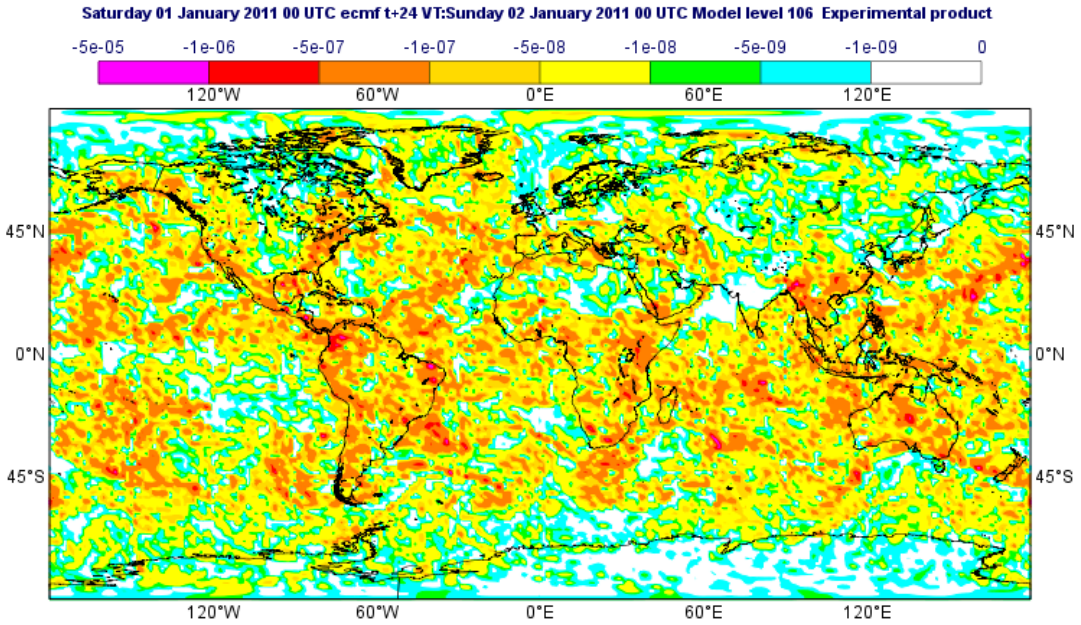

(a) PRqm fixer increment

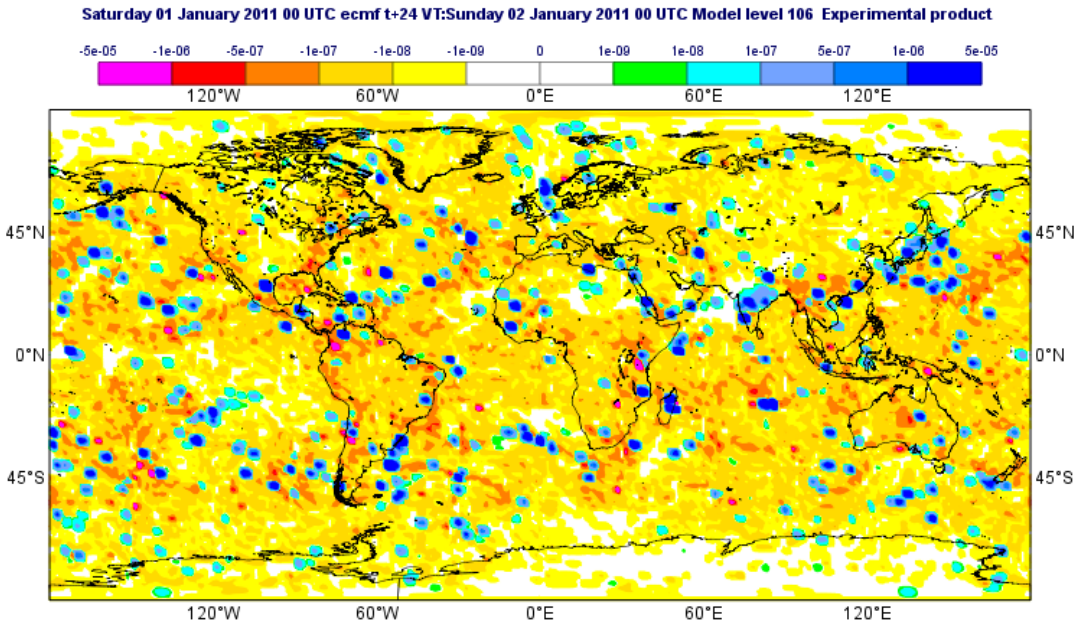

(b) PR fixer increment

Figure 4: PRqm and PR fixer Q increment at t+24 and 700 hPa height from a T1279 L137 forecast.

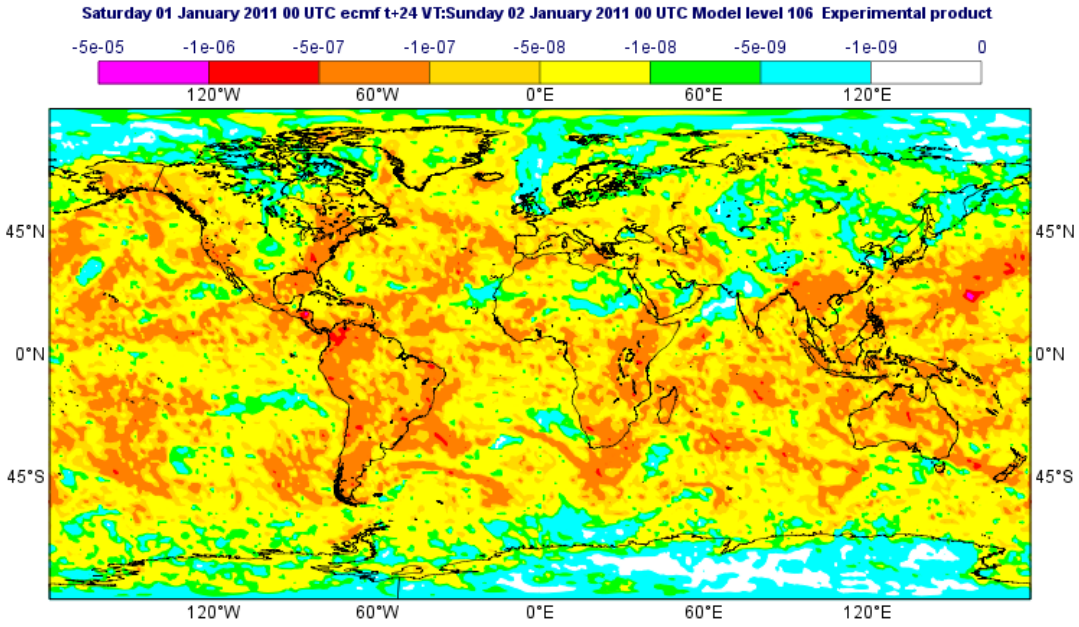

(a) ZE fixer

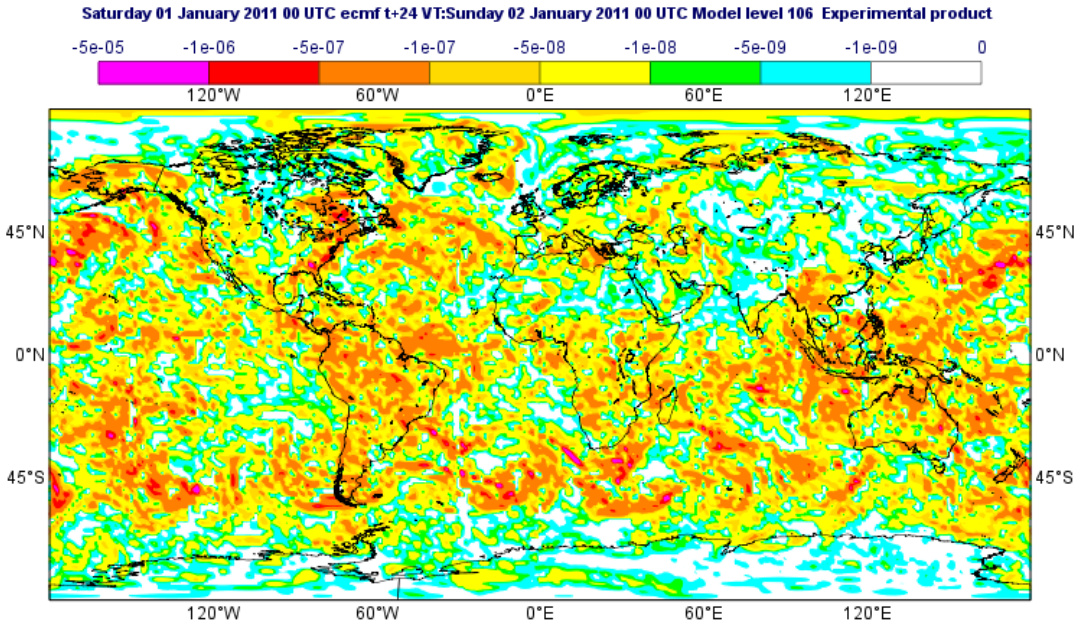

(b) JMG fixer

Figure 5: ZE and JMG fixer Q increment at t+24 and 700 hPa height from a T1279 L137 forecast.

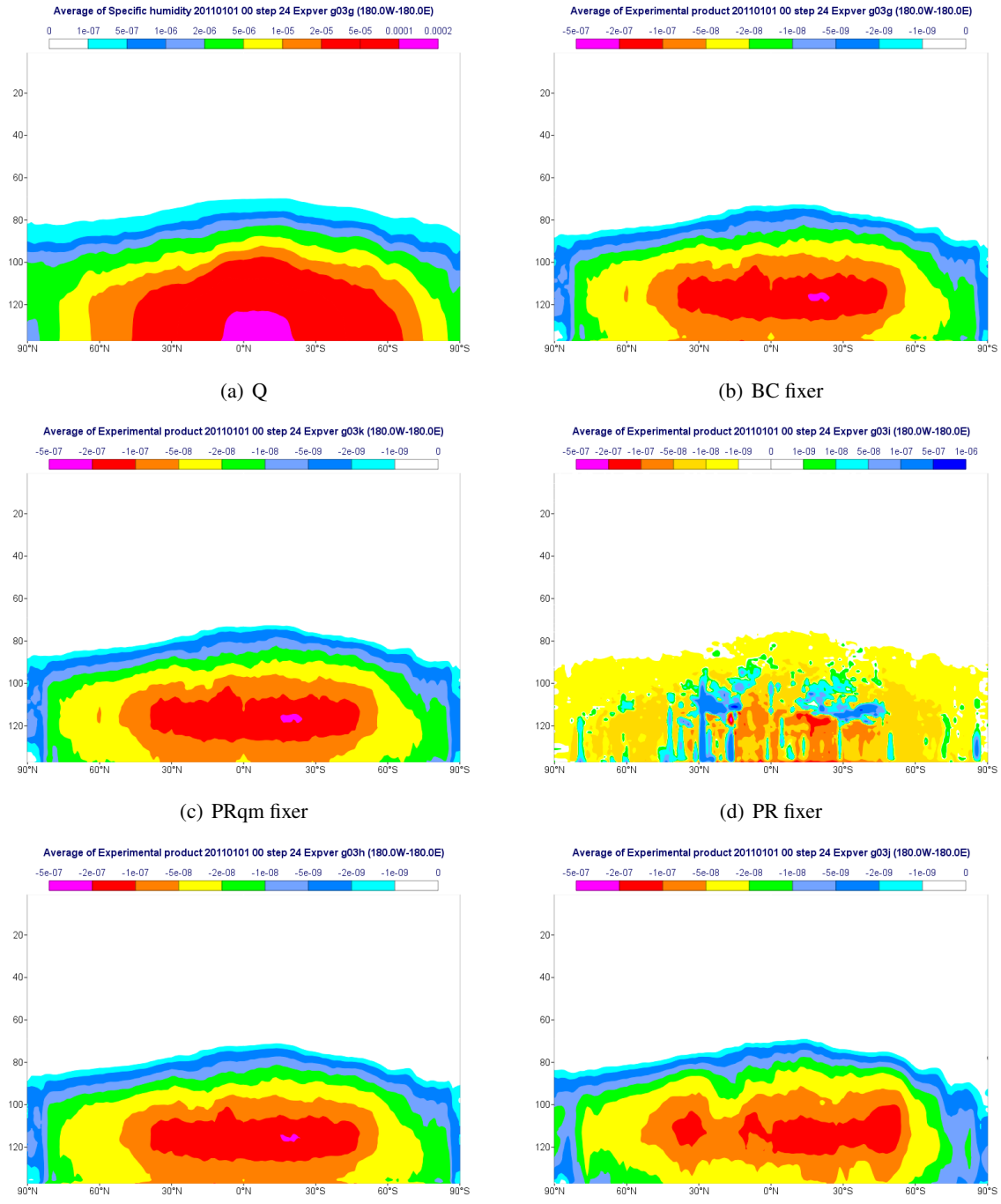

(a) Q (b) BC fixer

(c) PRqm fixer (d) PR fixer

(e) Ze fixer (f) JMG fixer

Figure 6: Time averaged (24 hrs) zonal mean of vertical cross sections for Q (a) and different mass fixer increments (b-f).

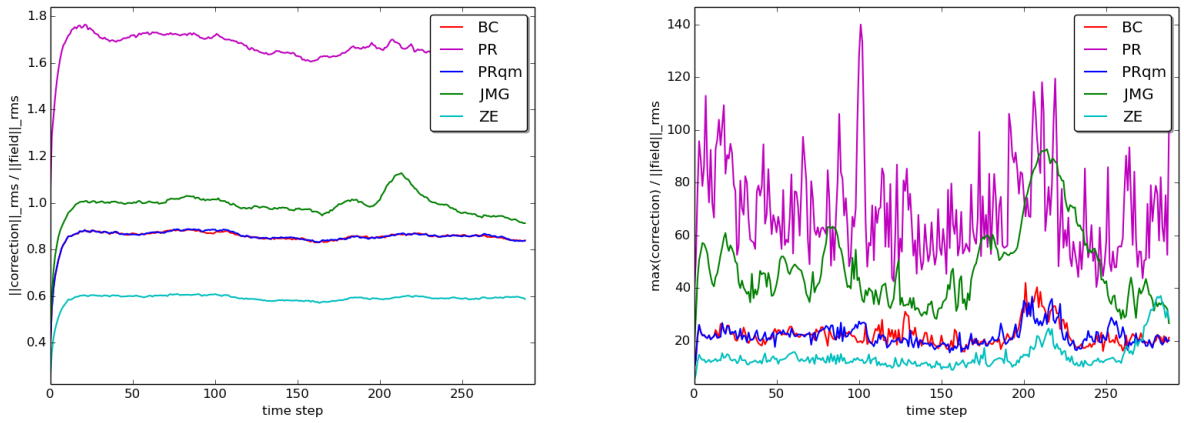

(a) $100 \times \|\delta\phi\|_{rms} / \|\phi\|_{rms}$ (%)

(b) $100 \times \max_j \{|\delta\phi_j|\} / \|\phi\|_{rms}$ (%)

Figure 7: 48 hrs timeseries of global rms-norms (left) and max-norms (right) of mass fixers increments for CLWC expressed as a percentage of the rms-norm of the field.

Mass Fixer	CPU overhead
BC	1%
PRqm	2%
PR	3.5%
JMG	0.75%
ZE	0.85%

Table 1: CPU overhead for different mass fixers in a 10 day forecast for the high resolution control T1279 L137.

4.1 Validation in long integrations

To assess the impact of fixers on long integrations, IFS has been tested on "climate case studies". This is simply a set of four 12-month long IFS forecasts with full physics at T159 L137 resolution. It is a standard test of IFS which is done to evaluate whether a new scheme impacts on model climate. The experiments run are described in Table 2.

In Fig. 8a the temperature bias is plotted, i.e. the difference of the vertical cross section of a zonally meaned and time averaged temperature field from its corresponding field from ERA-Interim run (taken as the "true" solution). Temperature is an appropriate diagnostic to measure the impact of the fixers given that altering the humidity content of the atmosphere will have a direct impact on temperature. This plot displays a common problem in semi-Lagrangian models, the extratropical tropopause/lower stratosphere cold bias Stenke et al. (2008). For the remaining plots, the difference of the same field (zonally meaned, time averaged temperature vertical cross section) from the control run is used. This is done to clearly demonstrate the impact of the changes. As a general rule, warming around the extratropical tropopause (in the region where the blue area in Fig. 8a appears) would indicate an improvement while cooling would indicate further deterioration.

Experiment	Description
control	operational setup: default quasi-monotone cubic interpolation on Q, linear interpolation on CLWC, CIWC, CRWC, CSWC (no fixer)
[control, JMG]	operational setup adding **JMG** fixer
[cubic qm]	default quasi-monotone cubic on Q, CLWC, CIWC, CRWC, CSWC (no fixer)
[cubic qm, BC]	cubic qm setup adding **BC** fixer on above moist fields
[cubic BSqm]	cubic qm setup using **BS** limiter instead of default
[unfiltered cubic, PR]	pure cubic Lagrange for moist fields, quasi-monotone advection by **PR** algorithm on moist fields.
[cubic BSqm, BC]	cubic BSqm setup adding **BC** fixer on moist fields
[cubic BSqm, JMG]	cubic BSqm setup adding **JMG** fixer on moist fields
[cubic BSqm, ZE]	cubic BSqm setup adding **ZE** fixer on moist fields

Table 2: List of 12-month forecast experiments.

Results show that none of these fixers deteriorates the existing cold bias. When the fixers are combined with the default limiter the difference in the results is small. On the contrary a clear improvement, i.e. a reduction of the cold bias, can be noticed when they are combined with the **BS** limiter. This shows in Fig. 9a to 9e. Good results are obtained with the quasi-monotone algorithms **PR**[3] and **BC**. Bigger positive impact is obtained by fixers that do not guarantee quasi-monotonicity: **ZE** followed by **JMG**. However, the former generates negatives especially in the cloud fields which are rougher (3-5% of grid-points become negative after correction is applied). This is not the case for the latter where a negative fixer is built in.

[3] As condition in equation (8) shows **PR** fixer is limiting the solution using a similar scheme to **BS** limiter.

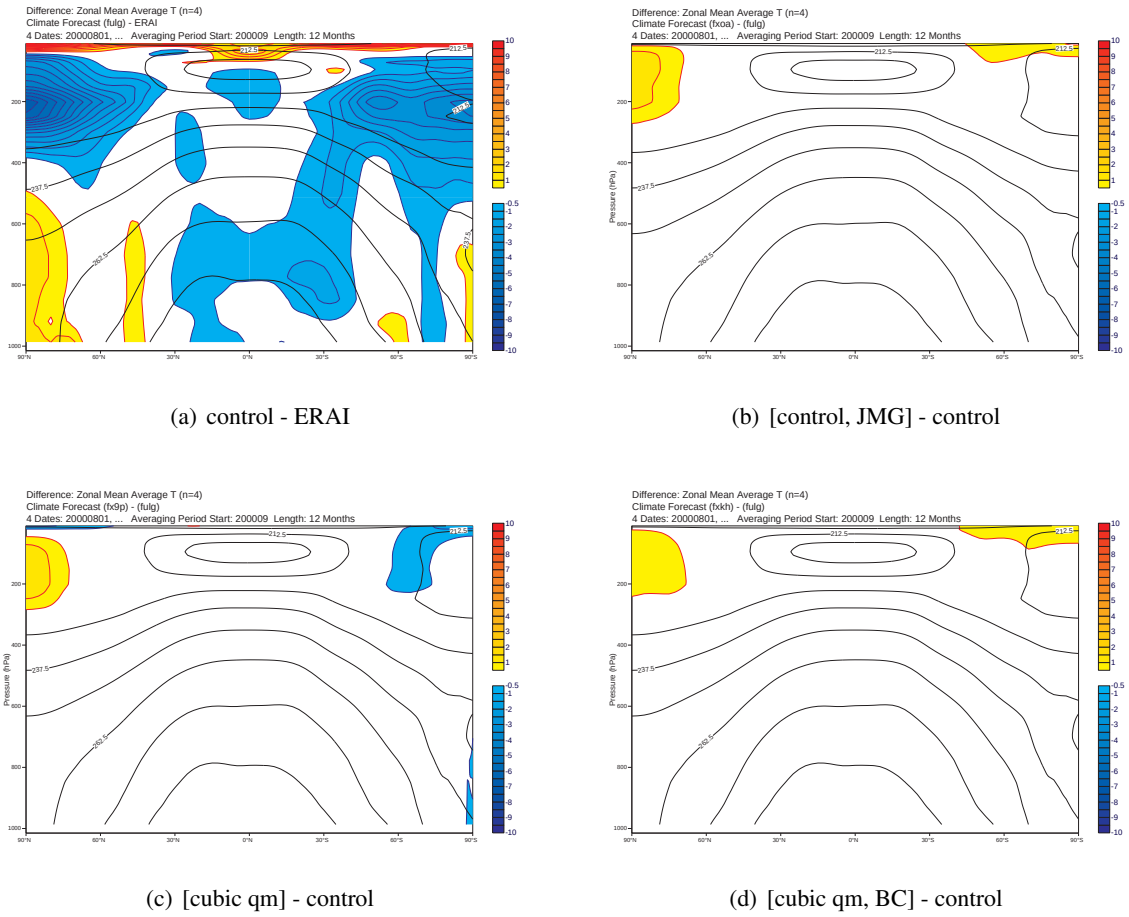

(a) control - ERAI

(b) [control, JMG] - control

(c) [cubic qm] - control

(d) [cubic qm, BC] - control

Figure 8: Simulations with default limiter. Difference of experiment's zonally-meaned, time-averaged vertical cross section of temperature field from ERA-Interim (top left) and from control forecast (remaining plots).

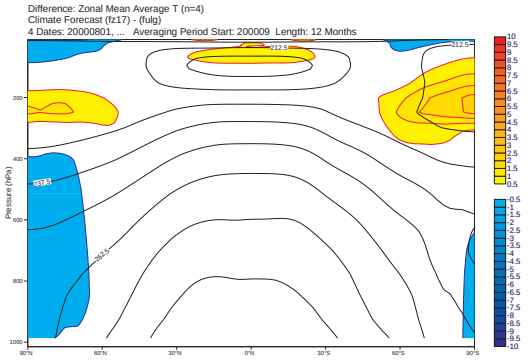

(a) [cubic BSqm] - control

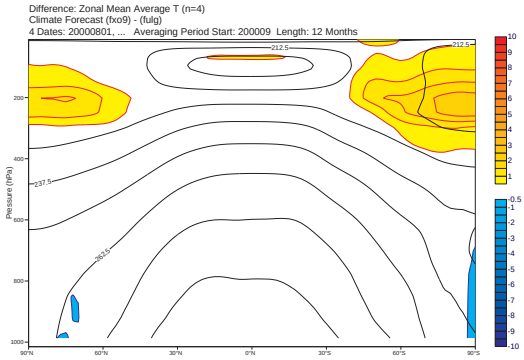

(b) [unfiltered cubic, PR] - control

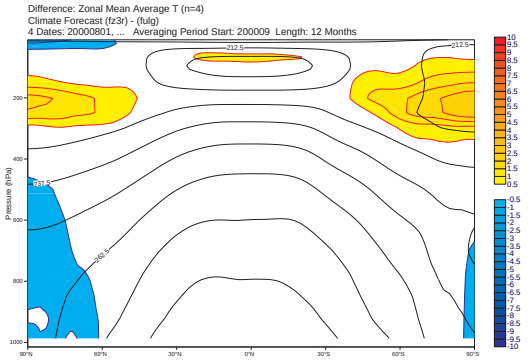

(c) [cubic BSqm, BC] - control

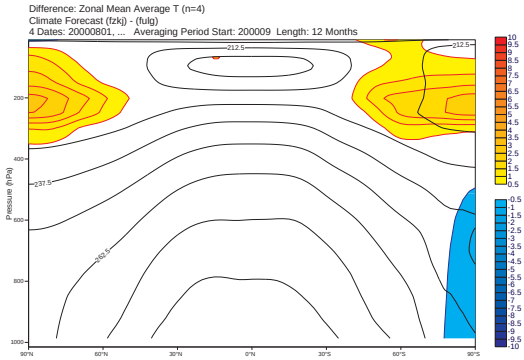

(d) [cubic BSqm, JMG] - control

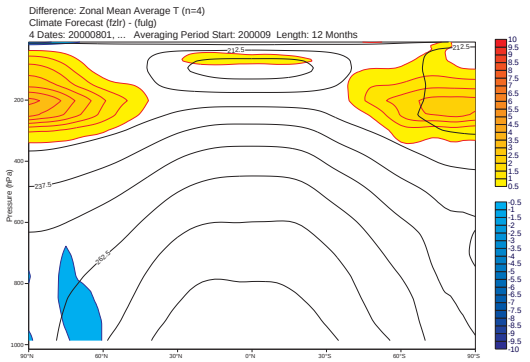

(e) [cubic BSqm, ZE] - control

Figure 9: Simulations with **BS** limiter. Difference of experiment's zonally-meaned, time-averaged vertical cross section of T-field from control forecast (ERAI for plot f).

4.2 Verification results

In general, it is not expected that a global mass fixer will improve forecasting skill in the short or medium range but neither it should deteriorate the skill. To investigate this the mass fixers have been tested on 37 forecast cases, each starting 10 days apart from 1/12/2011 until 25/11/2012. The resolution used is T511 L137 and each forecast is run for 10 days using operational options for the model dynamics and physics. All fixers were activated on Q, CLWC, CIWC, CRWC, CSWC. Although these tests are specific on moist physics tracers, they do have a general value. We can indirectly measure the impact a fixer has on advection by measuring the overall forecast skill of the experiment: forecast skill deterioration would imply that the tested algorithm deteriorates the accuracy of the advection scheme and therefore is deemed not suitable for tracer advection. Neutral scores should indicate that the fixer is making the interpolation conservative without damaging solution accuracy at least on the large scale.

Experiment	Description
control	operational setup: quasi-monotone cubic interpolation on Q, linear interpolation on CLWC, CIWC, CRWC, CSWC (no fixer)
[control, JMG]	operational setup adding **JMG** fixer
[cubic qm]	quasi-monotone cubic on Q, CLWC, CIWC, CRWC, CSWC (no fixer)
[cubic qm, BC]	cubic qm setup adding **BC** fixer on above moist fields
[cubic qm, ZE]	cubic qm setup adding **ZE** fixer on above moist fields
[unfiltered cubic, PR]	pure cubic Lagrange for moist fields, quasi-monotone advection by **PR** algorithm on moist fields

Table 3: List of T511L137 10-day forecast experiments.

The experiments run are summarized in Table 3. Overall, geopotential, wind, temperature diagnostics in the three global regions (NH, TR, SH) from these runs are neutral and there is no forecast that is better in terms of the usual statistical measures of ACC and RMSE. An exception is the temperature RMSE in the tropics at upper tropospheric levels which increases when any mass fixer is applied or when cubic quasi-monotone is used for CLWC, CIWC etc. The corresponding ACC scores remain neutral. This shows in Fig. 10 where ACC and RMSE results are indicatively plotted for the 500 hPa geopotential height field in the northern and southern hemisphere and for the 250 hPa temperature field in the tropics. Further analysis of the results shows that a small negative temperature bias in the control forecast in the tropical troposphere is slightly exaggerated (by 0.1 degrees at $t = 10$ days) when cubic interpolation is used for the cloud fields. The fixer contributes further (by a small amount) to this cooling. This happens because a small amount of humidity is removed from the atmosphere as a small humidity surplus is detected by the fixer. Reducing the humidity content of the troposphere has in general a cooling effect while the opposite is true for the stratosphere due to reduction of radiative cooling. The increase on RMSE is smaller when **JMG** fixer is used due to the fact that in this experiment it has been applied on linearly interpolated cloud fields (which gives better RMSE score). Tropical upper troposphere temperature scores are generally sensitive to small changes in moist field advection and parametrization tuning may be required to compensate.

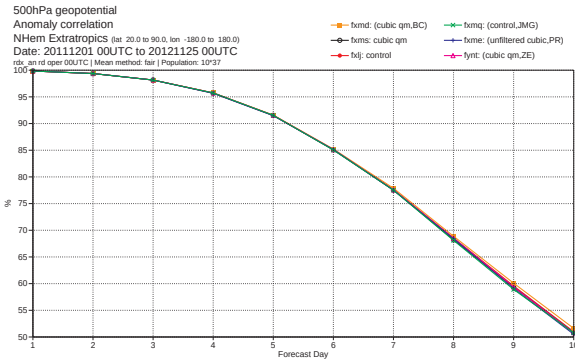

(a) NH 500 hPa geop ACC

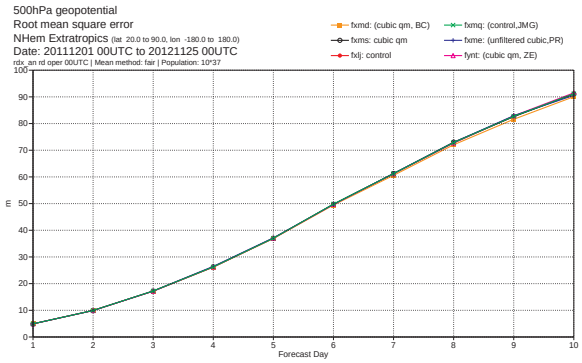

(b) NH 500 hPa geop RMSE

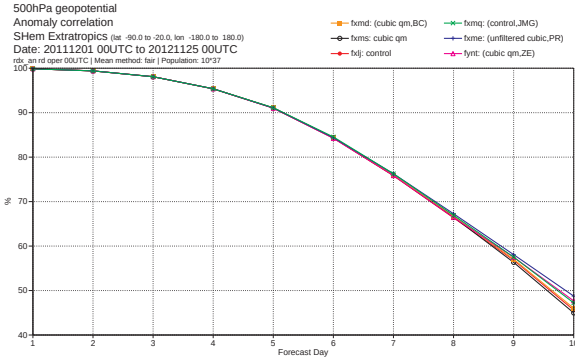

(c) SH 500 hPa geop ACC

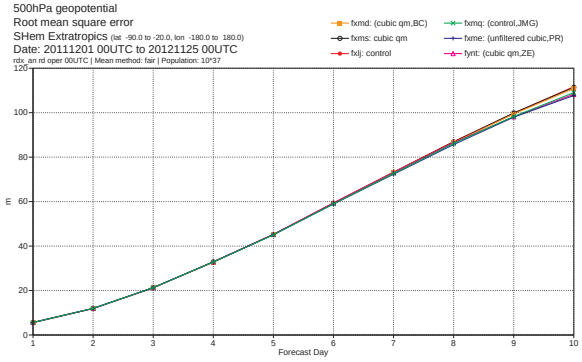

(d) SH 500 hPa geop RMSE

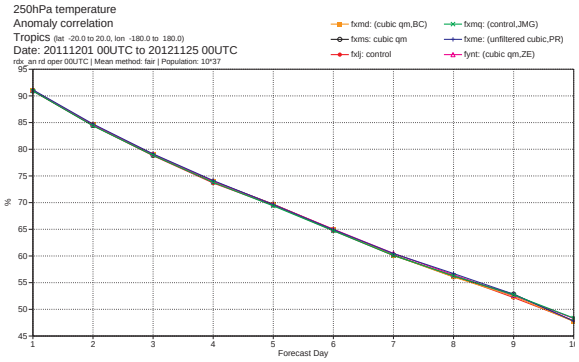

(e) TR 250hPa temperature ACC

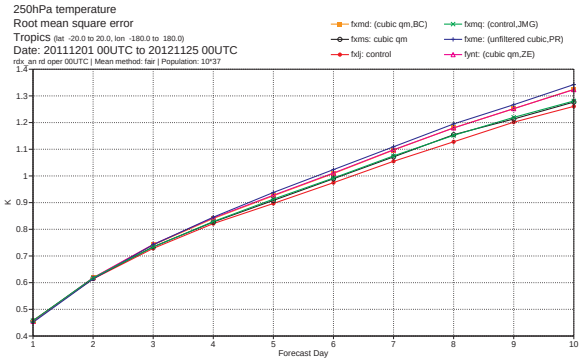

(f) TR 250hPa temperature RMSE

Figure 10: Northern and southern hemisphere ACC and RMSE for geopotential at 500 hPa. Temperature ACC and RMSE at 250 hPa in the tropics.

4.3 Simulation of correlated tracers case study

Mass conservation is an important property for atmospheric applications where chemical species are transported. It is additionally important that existing functional relationships in their concentration are maintained by the advection scheme (see Lauritzen and Thuburn, 2012). The ability of IFS and the newly developed fixers to preserve such relationships has been tested using case 11 from DCMIP (Dynamical Core Model Intercomparison Project, see Ulrich et al., 2012). This is a three-dimensional passive advection deformational flow idealised test case in which four tracers are transported. The initial concentration of the first two tracer fields q_1, q_2 obeys the nonlinear relationship:

$$q_2(\lambda,\theta,z) = 0.9 - 0.8q_1^2(\lambda,\theta,z)$$

where λ, θ, z is the longitude, latitude and height of a tracer. The first one (q_1) is represented by two cosine bells placed at the same height and latitude but at different longitudes.

Results for this test case from IFS runs at T159 horizontal resolution and 137 levels in the vertical[4] are plotted in Figs. 11, 12. The plots of Fig. 11 are correlation plots for the pair (q_1,q_2) at $t = 6$ days after the initial time. This is half the time required for the tracers to return to their original position i.e. complete one full rotation around the earth. The initial concentration of these tracers is given by the parabolic part of the dash-dotted black curve. Pairs (q_1,q_2) (red dots) that fall outside the region indicated by the dashed-dotted closed convex shape correspond to unphysical mixing ratios. Ideally, the red points should stay within the convex shape and follow the curve closely spreading evenly on it. Lack of spread indicates that the scheme is over-diffussive as peak values are damped. In Fig. 12, the initial concentration of the first tracer, $0 \leq q_1 \leq 1$, at a model level with height approximately equal to 5070m, is compared with its concentration at $t = 12$ days. Ideally, for a perfect advection scheme, the solution at $t = 0$ and $t = 12$ should be identical.

Inspection of these two plots show that semi-Lagrangian transport with linear interpolation is excessively diffusive but does not produce any unphysical mixing. The opposite is true when cubic Lagrange is used. It results in relatively large amount of unphysical mixing and overshoots/undershoots (new maxima/minima are created, see white areas in Fig. 12c corresponding to values above 1 and below 0). Significant improvements can be noticed when a quasi-monotone limiter is used. The default IFS limiter, being more strict (and damping) has big impact, all points stay inside the convex shape. However, maximum field values are damped. The **BS** limiter reduces but does not eliminate completely the unphysical mixing occurring with cubic interpolation. However, it preserves better the maxima (compare a, d and f in Fig. 12).

When a mass fixer is combined with the default IFS limiter it does not change further the mixing: it preserves equally well existing tracer correlations as shown in Fig. 11 (compare c and d). It also results in a small further reduction of maximum field values as we can see in Fig. 12. Better results are obtained when the fixers are combined with the **BS** limiter. In this case **BC** and **PR** produce the best results. They both preserve reasonably well the initial correlation (better than the corresponding run without fixer) and maximum field values are not too far from the analytical values. Finally, **ZE** and **JMG** fixers are not as effective in preserving the functional relationship (especially the latter) as a small proportion of points are outside the bounded sector. The former can produce undershoots (very small negatives) in some regions. However, they are both better in preserving maxima.

Concluding, according to the results obtained here, adding a mass fixer does not deteriorate the mixing properties of the advection scheme and in some occasions it may improve them. This is a desirable

[4]This horizontal and vertical resolution is close to the recommended for this problem.

result and suggests that mass fixers can be a beneficial addition for a semi-Lagrangian scheme used for transport of chemical tracers. Combination of a mass fixer with the **BS** limiter works better and **BC**, **PR** seem to give the best results.

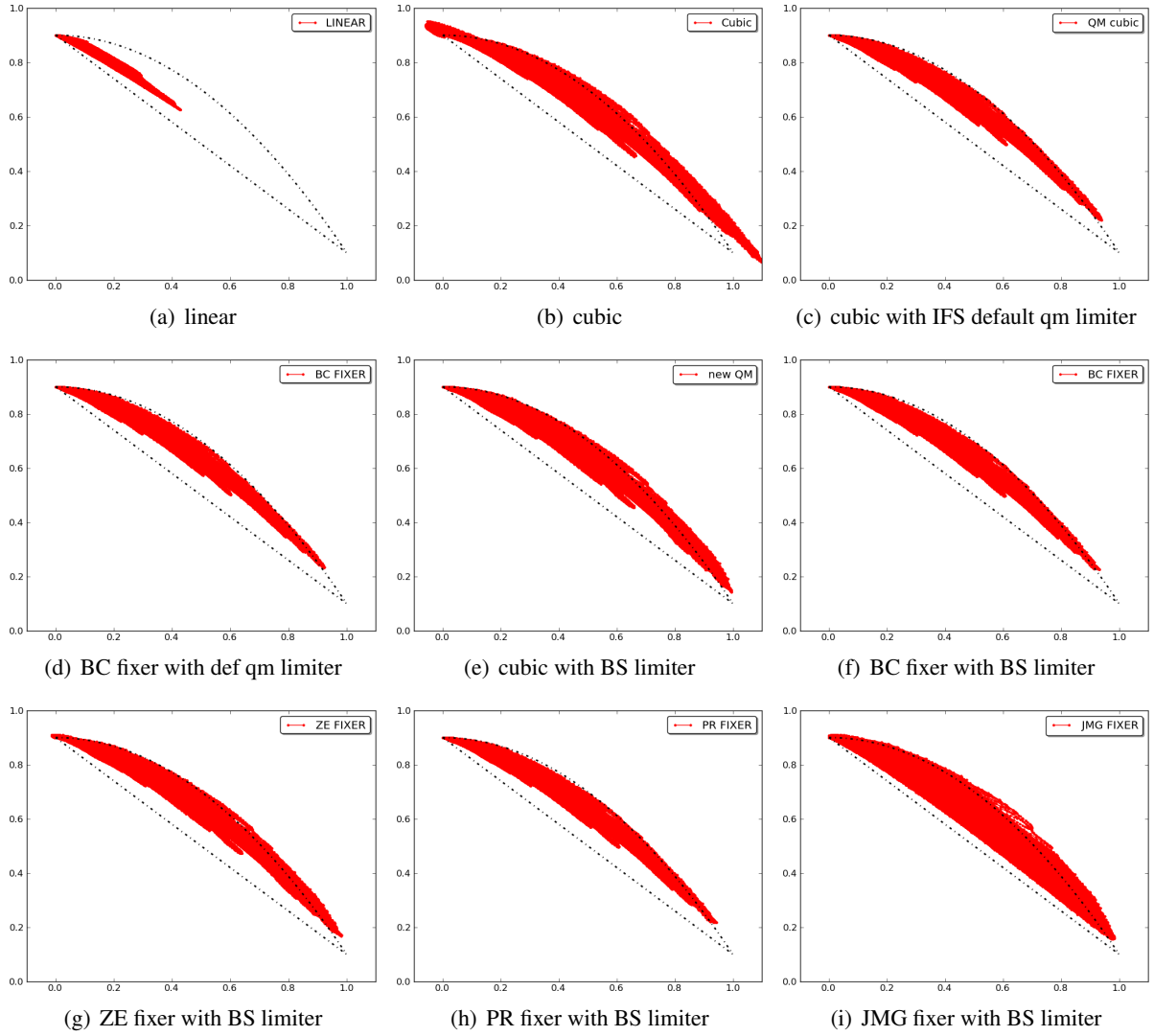

(a) linear (b) cubic (c) cubic with IFS default qm limiter

(d) BC fixer with def qm limiter (e) cubic with BS limiter (f) BC fixer with BS limiter

(g) ZE fixer with BS limiter (h) PR fixer with BS limiter (i) JMG fixer with BS limiter

Figure 11: q_1-q_2 (xy-axis) scatter plots for correlated tracers at $t = 6$ days. Scatter points (q_1,q_2) at $t = 0$ follow the upper black dashed-dotted curve.

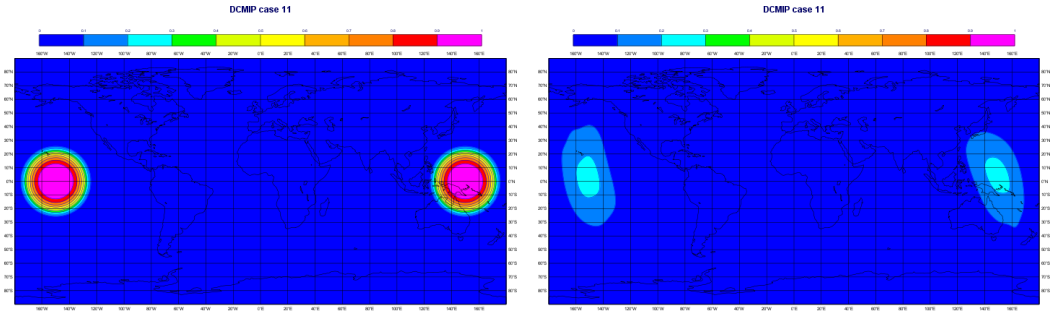

(a) $t = 0$ days: Initial concentration

(b) $t = 12$ days: linear interpol

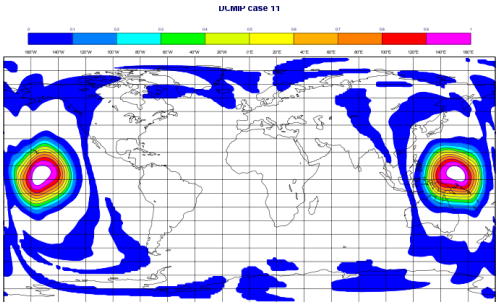

(c) $t = 12$ days: cubic

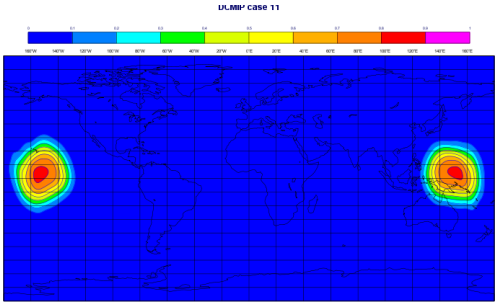

(d) $t = 12$ days: cubic + def qm limiter

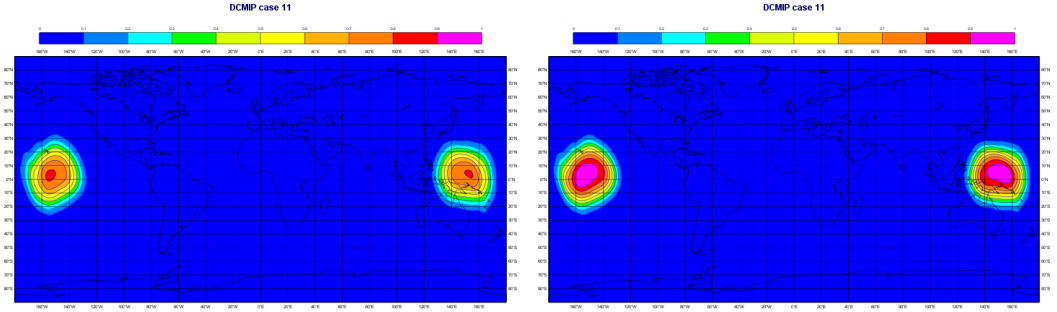

(e) $t = 12$ days: BC fixer + def qm

(f) $t = 12$ days: cubic + BS qm limiter

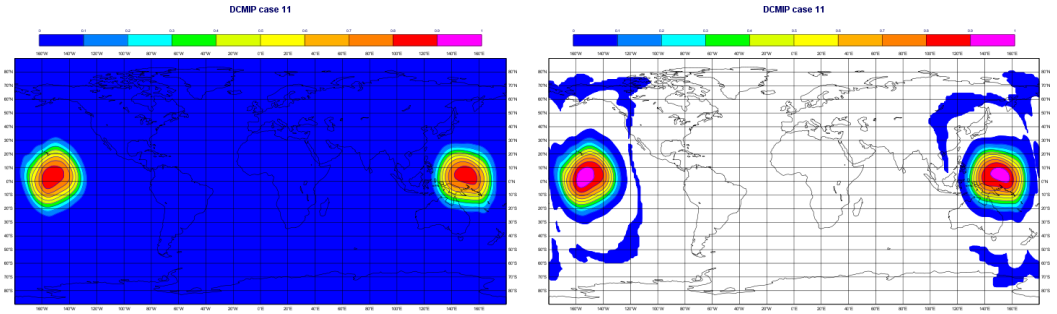

(g) $t = 12$ days: BC fixer + BS qm limiter

(h) $t = 12$ days: ZE fixer + BS qm limiter

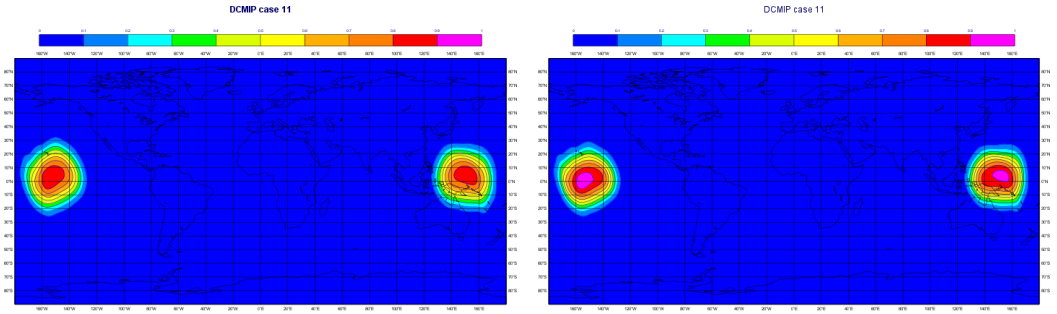

(i) $t = 12$ days: PR fixer

(j) $t = 12$ days: JMG fixer with BS limiter

Figure 12: Horizontal cross-section of tracer q_1 at $t = 12$ days and at 5070m height.

4.4 Volcanic plume case study

Mass fixers have also been tested on volcanic plume advection cases. Here a test case is presented where a tracer (SO2) is emitted into the atmosphere by a single point source and then transported by the winds. This case resembles the Grímsvötn volcanic eruption (see Flemming and Inness, 2013). Due to the highly localised nature of the advected plume, this case is a good test for assessing the local behaviour of a global mass fixer. The striking fact in this simulation is that the plume total mass is largely overestimated. A conservation error of almost 20% of the total mass of the field occurs during the first timesteps which eventually results to more than 50% gain. This is shown in Fig. 13. The greatly improved performance in terms of conservation error of the non-limited cubic Lagrange demonstrated in this plot is due to the presence of large negative undershoots which offset the overshoots when the global integral is computed and is therefore somewhat misleading.

Applying a mass fixer results in a globally conserving solution as shown by the 0 residual line in Fig. 13. It also results in some reduction of the peak values of the field which is evident in Fig. 14. This can be explained if we consider that a mass fixer diagnoses that the total mass has been largely overestimated by cubic interpolation and has to remove mass to enforce conservation. As the mass is concentrated in a small area, few grid-points across, peak values will be inevitably reduced when the mass fixer is applied. Large interpolation errors as a result of large gradients and insufficient resolution near the source is the main reason for this mass overestimation. The sensitivity with respect to the specific mass fixer or quasi-monotone filter used was relatively small and all algorithms tested behave in a similar way. The biggest difference was found between **JMG** fixer and the remaining ones and this shows in Fig. 14.

Although it is difficult to obtain accurate results in test cases of advection of small scale point sources with coarse (global) resolution semi-Lagrangian models, useful qualitative results can still be obtained. The mass fixer may reduce the amplitude of the field but it will correct its total mass which is necessary for emission parametric estimation.

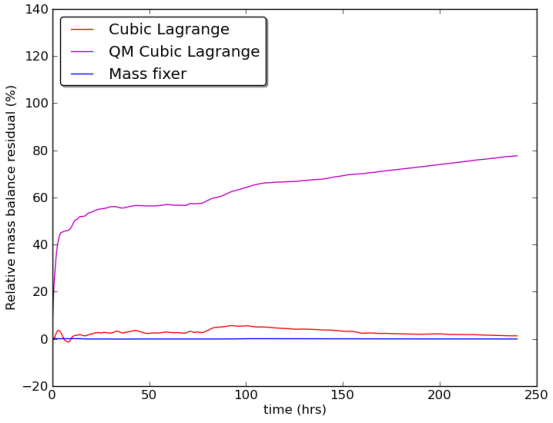

Figure 13: Mass Residual in volcanic plume simulations (SO2) for different schemes

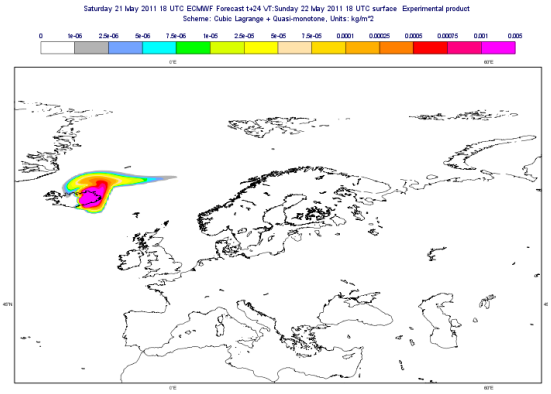

(a) cubic qm at $t = 24$ hrs

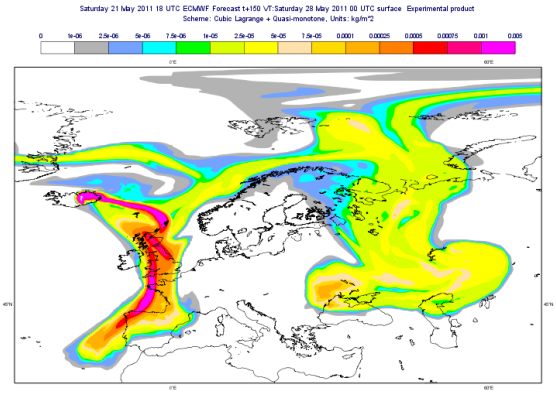

(b) cubic qm at $t = 150$ hrs

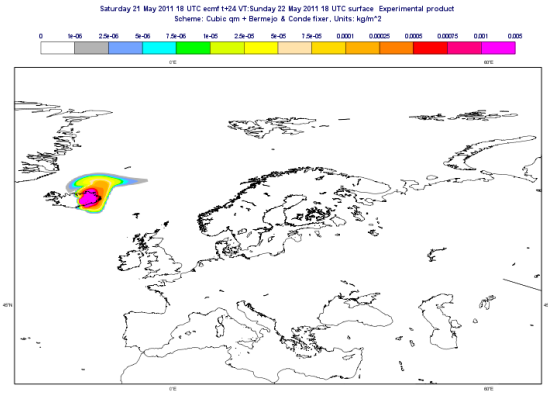

(c) cubic qm, BC fixer at $t = 24$ hrs

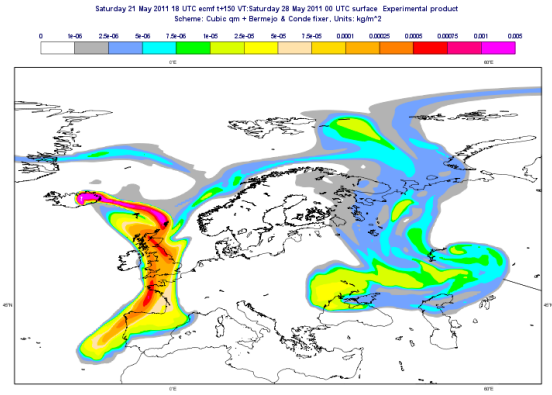

(d) cubic qm, BC fixer at $t = 150$ hrs

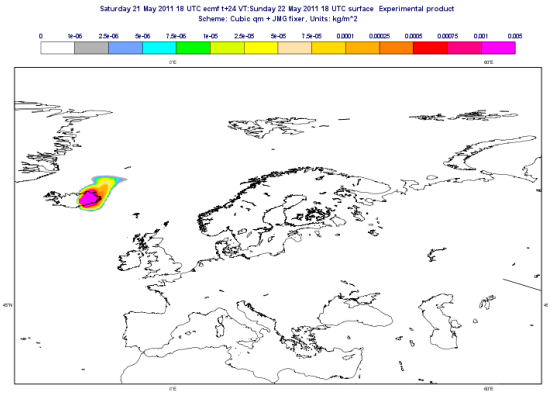

(e) cubic qm, JMG fixer at $t = 24$ hrs

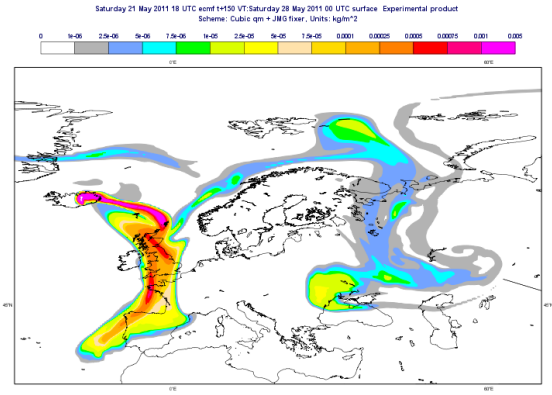

(f) cubic qm, JMG fixer at $t = 150$ hrs

Figure 14: Comparison of volcanic plume simulation with and without mass fixer using quasi-monotone cubic Lagrange at T1279 L91 resolution. The plotted quantity is the total SO2 content per model grid-point column.

5 Conclusions

A mass fixer is a technique to correct the global mass conservation error that a non-formally conserving advection scheme introduces. It acts in an a-posteriori fashion, corrects the solution after the field has been advected. In the context of a semi-Lagrangian scheme this means to correct the field after it has been interpolated to the departure point and before other source terms due to physical processes are added.

Different mass fixers have been recently implemented (cf. section 3) in IFS based on different strategies for correcting the global mass conservation error. They all follow a weighted approach, i.e. weights are computed which determine how much to adjust each grid-point value. The aim is to correct the advected field in regions where the interpolation error is large. Results show that indeed these methods act in areas of steep gradients where the solution is not smooth while they apply very small corrections elsewhere. They achieve globally mass conserving solutions without deteriorating accuracy at large scales. This has been demonstrated here by a set of 12-month forecast tests verified against ERA-Interim and standard 10 day forecasts at T511 L137 resolution verified against ECMWF operational analysis.

The key results from this work are:

1. No significant differences have been found between the approaches at the hydrostatic scales tested. But there are differences in cost.
2. Global conservation is achieved without deteriorating the solution. An exception is the volcanic plume case in which peak values are reduced. However, this side-effect is also related to the lack of sufficient resolution. Despite this, global mass conservation is important for emission parametric estimates.
3. The impact on forecast skill is neutral.
4. Big impact was found from the quasi-monotone limiter applied. In long integrations **BS** improves on the standard quasi-monotone scheme used in IFS.

Based on the above findings the recommendations on the use of the newly implemented mass fixers are:

1. Currently the **BC** fixer is recommended for simulations with chemical tracers because it is one of the cheapest and performs well in advecting correlated tracers (cf. Fig. 11).
2. For volcanic plumes, **BC** is also sufficient.
3. For "standard" advection options of moist quantities in IFS (quasi-cubic, quasi-monotone interpolation for specific humidity, linear for cloud fields), the cheapest fixer **JMG** is sufficient. It is the only one that can be applied for advection with linear interpolation.
4. For "cubic" advection of moist quantities (quasi-cubic, quasi-monotone for specific humidity and cloud fields) **BC** is the preferred option as it is shape preserving and one of the cheapest.

The general belief in the atmospheric modelling community is that mass fixers may be inappropriate at non-hydrostatic, cloud-resolving scales. Future tests will include these regimes. On going developments in the PantaRhei project (ECMWF, 2013) will provide opportunities towards a strictly mass-conserving scheme in this regime. Until such developments materialise, mass fixers can provide a practical alternative for the applications supported by IFS and are attractive due to their low computational cost.

Acknowledgements

The authors wish to thank Dr S. Malardel for providing her idealised case study code and useful advice for this work.

The authors also gratefully acknowledge the help of Prof. E. Källén and Dr N. Wedi who provided constructive review comments on this manuscript.

A Activating mass fixers in IFS

In Table 4 an example is given where **JMG** fixer is activated through NAMGFL namelist options. A description of these arguments as well as of all the available control variables related to mass fixers is given in Table 6. These options should be valid for model cycles 39r1 and later. Statistical diagnostics, printed in the output file, corresponding to the setup of Table 4 is given in Table 5.

```
LTRCMFIX=true,
LTRCMFMG=true,
NOPTVFE=1,
NMFDIAGLEV=2,
YL_NL%%LINTLIN=false,
YI_NL%%LINTLIN=false,
YR_NL%%LINTLIN=false,
YS_NL%%LINTLIN=false,
YL_NL%%LQM=true,
YI_NL%%LQM=true,
YR_NL%%LQM=true,
YS_NL%%LQM=true,
YQ_NL%%LMASSFIX=true,
YL_NL%%LMASSFIX=true,
YI_NL%%LMASSFIX=true,
YR_NL%%LMASSFIX=true,
YS_NL%%LMASSFIX=true,
```

Table 4: Mass fixers NAMGFL namelist control options.

```
 ------------------------------------------------------------------------------
                  MASS FIXER GLOBAL DIAGNOSTICS
     FIELD         DM       DM/Mtot %    max(dij)/|field| %   |dij|/|field| %
------------------------------------------------------------------------------
     HUMIDITY  0.7504E-03     0.003           0.073               0.005
 LIQUID WATER  0.2534E-03     0.435          44.991               0.825
   ICE WATER   0.5047E-04     0.204          19.012               0.398
        SNOW   0.5105E-04     0.085           8.780               0.177
        RAIN   0.7591E-05     0.063          10.413               0.128
CLOUD FRACTI   0.1338E+01     0.175           1.889               0.380
 SUB JMGFIXER() - FLD:      HUMIDITY  FIXER UNDERSHOOTS MINIMUM AT   8328 POINTS!
 UNDERSHOOTS AT    0.00% OF POINTS
 SUB JMGFIXER() - FLD:  LIQUID WATER  FIXER UNDERSHOOTS MINIMUM AT   6775 POINTS!
 UNDERSHOOTS AT    0.00% OF POINTS
 SUB JMGFIXER() - FLD:     ICE WATER  FIXER UNDERSHOOTS MINIMUM AT   3808 POINTS!
 UNDERSHOOTS AT    0.00% OF POINTS
 SUB JMGFIXER() - FLD:          SNOW  FIXER UNDERSHOOTS MINIMUM AT   3910 POINTS!
 UNDERSHOOTS AT    0.00% OF POINTS
 SUB JMGFIXER() - FLD:          RAIN  FIXER UNDERSHOOTS MINIMUM AT   6777 POINTS!
 UNDERSHOOTS AT    0.00% OF POINTS
 SUB JMGFIXER() - FLD:  CLOUD FRACTI  FIXER UNDERSHOOTS MINIMUM AT  52596 POINTS!
 UNDERSHOOTS AT    0.03% OF POINTS
```

Table 5: Fixer diagnostic output corresponding to namelist in Table 4 where NMFDIAGLEV=2

FLAG (default)	**DESCRIPTION**
LTRCMFIX (F)	LOGICAL: mass fixers generic flag - should be true for activating any of them.
LTRCMFBC (F)	LOGICAL: if true activate BC fixer.
LTRCMFPR (F)	LOGICAL: if true activate PR or PRqm fixer.
LTRCMFMG (F)	LOGICAL: if true activate JMG fixer.
NOPTMFIX (1)	INTEGER: applies only to settings LTRCMFBC=true and LTRCMFPR=true if LTRCMFBC=T & NOPTMFIX=1 use BC fixer if LTRCMFBC=T & NOPTMFIX=2 use Ze version if LTRCMFPR=T & NOPTMFIX=1 use PRqm fixer if LTRCMFPR=T & NOPTMFIX=2 use PR fixer.
NOPTVFE (0)	INTEGER: if NOPTVFE=0 compute total column mass using finite-difference approximation. if NOPTVFE=1 compute total column mass using finite-element approximation.
NMFDIAGLEV (0)	Level of diagnostic output. This is written in the output file of each forecast. An example for NMFDIAGLEV=2 is shown in Table 5. if NMFDIAGLEV=0: no extra diagnostic output generated. if NMFDIAGLEV=1: global statistics are generated at each timestep showing: DM: mass gain (positive) or loss (negative) DM/Mtot: percentage of mass gain/loss DM wrt total mass Mtot max(dij)/|field|: max-norm of fixer increment absolute value expressed as a percentage of global rms-norm of the field that corrects |dij|/|field|: rms-norm of fixer increment expressed as a percentage of global rms-norm of the field that corrects if NMFDIAGLEV=2: in addition to NMFDIAGLEV=1 diagnostics print shape preservation violations (over/under shoots)
	RELEVANT FLAGS IN YOM_GFL TYPE e.g. YQ_NL%%<FLAG>
LMASSFIX (F)	LOGICAL: applied to advected GFL - if true then mass fixer will be applied on this GFL
LINTLIN	LOGICAL: applied to advected GFL -if true use linear interpolation. Default values depend on GFL variable.
LQM	LOGICAL: applied to advected GFL -if true and LINTLIN=false use quasi-monotone cubic Lagrange interpolation. Default values depend on GFL variable. and LINTLIN=false then use BS limiter in cubic Lagrange interpolation.

Table 6: Description of control variables for mass fixers valid for cycles up to 40r1

References

Bermejo, R. and J. Conde (2002). A conservative quasi-monotone semi-Lagrangian scheme. *Mon. Weather Rev. 130*, 423–430.

Bermejo, R. and A. Staniforth (1992). The conversion of semi-Lagrangian advection schemes to quasi-monotone schemes. *Mon. Weather Rev. 120*, 2622–2631.

ECMWF (2013). EU PantaRhei Project at ECMWF. http://www.ecmwf.int/research/EU_projects/PANTARHEI/index.html.

ECMWF, R.-D. (2012). IFS documentation. http://www.ecmwf.int/research/ifsdocs/.

Flemming, J. and A. Inness (2013). Volcanic sulphur dioxide plume forecasts based on UV-satellite retrievals for the 2011 Grímsvötn and the 2010 Eyjafjallajokull eruption. *J. Geophys. Res. 118*, 172–189.

Gravel, S. and A. Staniforth (1994). A mass-conserving semi-Lagrangian scheme for the shallow-water equations. *Mon. Weather Rev. 122*, 243–248.

Lauritzen, P., R. D. Nair, and P. A. Ullrich (2010). A conservative semi-Lagrangian multi tracer transport scheme (CSLAM) on the cubed-sphere grid. *J. Comput. Phys. 229*, 1401–1424.

Lauritzen, P. and J. Thuburn (2012). Evaluating advection/transport schemes using interrelated tracers, scatter plots and numerical mixing diagnostics. *Q.J.R. Meteorol. Soc. 138*, 906–918.

MacGregor, J. (2011). C-CAM geometric aspects and dynamical formulation. Technical Report 70, CSIRO Atmospheric Research, Aspendale, Vic.

Priestley, A. (1993). A quasi-conservative version of the semi-Lagrangian advection scheme. *Mon. Weather Rev. 121*, 621–629.

Rasch, P. and D. Williamson (1990). Computational aspects of moisture transport in global models of the atmosphere. *Q.J.R. Meteorol. Soc. 116*, 1071–1090.

Ritchie, H. and M. Tanguay (1996). A comparison of spatially averaged Eulerian and semi-Lagrangian treatment of mountains. *Mon. Weather Rev. 124*, 167–181.

Ritchie, H., C. Temperton, A. Simmons, M. Hortal, T. Davies, D. Dent, and M. Hamrud (1995). Implementation of the semi-Lagrangian method in a high-resolution version of the ECMWF forecast model. *Mon. Weather Rev. 121*, 489–514.

Sørensen, B., E. Kaas, and U. Korsholm (2013). A mass-conserving and multi-tracer efficient transport scheme in the online integrated enviro-hirlam model. *Geosci. Model Dev. 6*, 1029–1042.

Stenke, A., V. Grewe, and M. Ponater (2008). Lagrangian transport of water vapor and cloud water in the ECHAM4 GCM and its impact on the cold bias. *Clim Dyn 31*, 491–506.

Ulrich, P., C. Jablonowski, J. Kent, P. Lauritzen, R. Nair, and M. Taylor (2012). Dynamical Core Model Intercomparison Project (DCMIP) test case document. Technical report, NCAR.

Zerroukat, M. (2010). A simple mass conserving semi-Lagrangian scheme for transport problems. *J. Comput. Phys. 229*, 9011–9019.

Zerroukat, M. and T. Allen (2012). A three-dimensional monotone and conservative semi-Lagrangian scheme (SLICE-3D) for transport problems. *Q.J.R. Meteorol. Soc. 138*, 1640–1651.